

Variation of fluorescence spectroscopy during the menstrual cycle

Calum MacAulay

*British Columbia Cancer Research Centre, 601 West 10th Avenue, Vancouver, British Columbia V5Z 1L3, Canada
cmacula@bccancer.bc.ca*

Rebecca Richards-Kortum, Urs Utzinger

*The Dept. of Electrical and Computer Engineering and The Biomedical Engineering Program, ENS 610 The
University of Texas, Austin, TX 78712
kortum@mail.utexas.edu*

Amanda Fedyk

*British Columbia Cancer Research Centre, 601 West 10th Avenue, Vancouver, British Columbia V5Z 1L3, Canada
afedyk@bccancer.bc.ca*

E. Neely Atkinson

*Dept. of Biomathematics, The University of Texas M.D. Anderson Cancer Center, 1515 Holcombe Blvd., Houston, TX
77030
eatkinso@mdanderson.org*

Dennis Cox

*Dept. of Statistics, Rice University, 6100 S. Main Street, Houston, TX 77030
dcx@stat.rice.edu*

Michele Follen

*Dept. of Gynecologic Oncology, The University of Texas M.D. Anderson Cancer Center, 1515 Holcombe Blvd.,
Houston, TX 77030
mfollen@mdanderson.org*

Abstract: Cervical autofluorescence has been demonstrated to have potential for real-time diagnosis. Inter-patient and intra-patient variations in fluorescence intensity have been measured. Inter-patient measurements may vary by a factor of ten, while intra-patient measurements may vary by a factor of two. Age and menopausal status have been demonstrated to account for some of the variations, while race and smoking have not. In order to explore in detail the role of the menstrual cycle in intra-patient variation, a study was designed to measure fluorescence excitation emission matrices (EEMs) in patients daily throughout one cycle. Ten patients with a history of normal menstrual cycles and normal Papanicolaou smears underwent daily measurements of fluorescence EEMs from three colposcopically normal sites throughout one menstrual cycle. Changes in signals from porphyrin, NADH, and FAD fluorescence and blood absorption were noted when the data was viewed in a graphical format. Visually interpreted features of the EEMs in this graphical format did not appear to correlate with the day of the menstrual cycle with the exception that blood absorption features were more prominent during the menstrual phase (during which bleeding occurs), suggesting that measurements during the menstrual phase should be avoided. Variations in cycle date likely do not account for inter- or intra-patient variations.

©2002 Optical Society of America

OCIS codes: (170.6280) Spectroscopy, fluorescence and luminescence;
(170.6510) Spectroscopy, tissue diagnostics

References and Links

1. I. J. Bigio, T. R. Loree, J. Mourant, "Spectroscopic diagnosis of bladder cancer with elastic light scattering," *Lasers Surg Med* **16**, 350-357 (1995).
2. L. Perelman, V. Backman, M. Wallace, G. Zonios, R. Manoharan, A. Nusrat, S. Shields, M. Seiler, C. Lima, T. Hamano, I. Itzkan, J. Van Dam, J. M. Crawford, M. S. Feld, "Observation of periodic fine structure in reflectance from biological tissue: a new technique for measuring nuclear size distribution," *Phys Rev Lett* **80**, 627-30 (1998).
3. R. R. Alfano, G. C. Tang, A. Pradham, W. Lam, D. S. J. Choy, E. Opher, "Fluorescence spectra from cancerous and normal human breast and lung tissues," *IEEE J Quant Electron* **23(10)**, 1806-1811 (1987).
4. J. Hung, S. Lam, J. C. LeRiche, B. Palcic, "Autofluorescence of normal and malignant bronchial tissue," *Lasers Surg Med* **11**, 99-105 (1991).
5. R. Richards-Kortum, R. P. Rava, R. E. Petras, M. Fitzmaurice, M. Sivak, M. S. Feld, "Spectroscopic diagnosis of colonic dysplasia," *Photochem Photobiol* **53(6)**, 777-786 (1991).
6. K. T. Schomacker, J. K. Frisoli, C. Compton, "Ultraviolet laser-induced fluorescence of colonic tissue: Basic biology and diagnostic potential," *Lasers Surg Med* **12**, 63-78 (1992).
7. S. Lam, C. MacAulay, J. Hung, J. LeRiche, A. E. Profio, B. Palcic, "Detection of dysplasia and carcinoma *in situ* with a lung imaging fluorescence endoscope device," *J Thoracic Cardiovasc Surg* **105**, 1035-40 (1993).
8. H. Zeng, D. I. McLean, C. MacAulay, H. Lui, "Autofluorescence properties of skin and applications in dermatology," *Proc SPIE* **4224**, 366-373 (2000).
9. U. Utzinger, D. L. Heintzelman, A. Mahadevan-Jansen, A. Malpica, M. Follen, R. Richards-Kortum, "Near infrared Raman spectroscopy for *in vivo* detection of cervical precancers," *Appl Spectrosc*, **5**, 955-959 (2001).
10. M. Rajadhyaksha, D. Grossman, R. Esterowitz, H. Webb, R. Anderson, "In vivo confocal scanning laser microscopy of human skin: melanin provides strong contrast," *J Invest Dermatol* **104**, 946-952 (1995).
11. C. Smithpeter, A. Dunn, R. Drezek, T. Collier, R. Richards-Kortum, "Near real time confocal microscopy of *in situ* amelanotic cells: sources of signal, contrast agents, and limits of contrast," *J Biomed Opt* **3**, 429-43 (1998).
12. S. A. Boppart, J. M. Herrmann, C. Pitris, D. L. Stamper, M. E. Brezinski, J. G. Fujimoto, "Real-time optical coherence tomography for minimally invasive imaging of prostate ablation," *Comput Aided Surg* **6(2)**, 94-103 (2001).
13. J.M. Poneros, S. Brand, B.E. Bouma, G.J. Tearney, C.C. Compton, N.S. Nishioka, "Diagnosis of specialized intestinal metaplasia by optical coherence tomography," *Gastroenterology* **120(1)**:7-12.
14. N. Ramanujam, M. F. Mitchell, A. Mahadevan, S. Thomsen, E. Silva, R. R. Richards-Kortum, "In vivo diagnosis of cervical intraepithelial neoplasia using 337 nm laser induced fluorescence," *Proc Natl Acad Sci U S A* **91**, 10193-97 (1994).
15. N. Ramanujam, M. Follen Mitchell, A. Mahadevan, S. Thomsen, A. Malpica, T. Wright, N. Atkinson, R. Richards-Kortum, "Spectroscopic diagnosis of cervical intraepithelial neoplasia (CIN) *in vivo* using laser induced fluorescence spectra at multiple excitation wavelengths," *Lasers Surg Med* **19**, 63-74 (1996).
16. N. Ramanujam, M. Follen Mitchell, A. Mahadevan-Jansen, S. Thomsen, G. Staerker, A. Malpica, T. Wright, N. Atkinson, R. Richards-Kortum, "Cervical pre-cancer detection using a multivariate statistical algorithm based on laser induced fluorescence spectra at multiple excitation wavelengths" *Photochem Photobiol* **6**, 720-35 (1996).
17. C. Brookner, U. Utzinger, G. Staerker, R. Richards-Kortum, M. F. Mitchell, "Cervical fluorescence of normal women," *Lasers Surg Med* **24**, 29-37 (1999).
18. C. Brookner, U. Utzinger, M. Follen, R. Richards-Kortum, E. N. Atkinson, "Effects of biographical variables on cervical fluorescence emission spectra," submitted, *J Biomed Opt* (2001).
19. A. Zuluaga, U. Utzinger, A. Durkin, H. Fuchs, A. Gillenwater, R. Jacob, B. Kemp, J. Fan, R. Richards-Kortum, "Fluorescence excitation emission matrices of human tissue: a system for *in vivo* measurement and data analysis," *Appl Spectrosc* **53**, 302-311 (1999).
20. D. D. Cox, S. K. Chang, M. Y. Dawood, G. Staerker, U. Utzinger, R.R. Richards-Kortum, M. Follen, "Detecting the signal of the menstrual cycle in fluorescence spectroscopy of the cervix," submitted, *Appl Spectrosc* (2001).
21. M. Bueeler, "Design Optimization and Quality Control of a Fluorescence and Reflectance Spectroscopy System," Diploma Thesis, Dept. of Biomedical Engineering, Swiss Federal Institute of Technology, Zurich (2000).
22. S. K. Chang, M. Y. Dawood, G. Staerker, U. Utzinger, R. R. Richards-Kortum, M. Follen, "Fluorescence spectroscopy for cervical pre-cancer detection: is there variance across the menstrual cycle?" submitted, *J Biomed Opt* (2001).

1. Introduction

Emerging optical technologies can provide real-time, *in vivo* diagnosis of invasive and non-invasive epithelial neoplasia. These technologies are enabling novel cancer-control strategies that exploit the real-time detection and localization of early cancers and precancerous tissue capabilities. A number of groups have examined novel optical approaches, including

reflectance spectroscopy [1,2], fluorescence spectroscopy [3-6], fluorescence imaging [7,8], Raman spectroscopy [9], confocal imaging [10,11], and optical coherence tomography [12,13]. Of all these optical technologies the use of fluorescence spectroscopy for neoplasia detection and localization has seen the most clinical experience in the largest variety of tissue types.

The preeminently successful cancer management program through the detection of non-invasive neoplasia and its treatment is that of cervical Pap screening and colposcopic follow-up. Many of these optical technologies—fluorescence spectroscopy in particular—have the potential to be beneficially incorporated into this cancer management program if they can be shown to have robust detection and localization properties.

Fluorescence spectroscopy has been demonstrated to have a sensitivity and specificity of 86% and 74% in the diagnostic colposcopy clinic and 75% and 80% in the screening setting [14-17]. In both diagnostic and screening settings, inter-patient variability of approximately an order of magnitude has been noted. In an attempt to further improve the sensitivity and specificity of real-time diagnosis, it is necessary to understand and control for the sources of this inter-patient variability. Previous work has shown that race and smoking do not account for these variations, while age, menopausal status, and phase in the menstrual cycle may play a role [18]. To examine the influence of age on fluorescence spectroscopy we are currently conducting large clinical trials in diagnostic and screening settings. In the study presented here we examine the variations in fluorescence spectra throughout the menstrual cycle for a set of ten volunteers.

2. Methods

2.1 Patient Measurements

The study protocol was reviewed and approved by the Institutional Review Boards at the University of Texas M. D. Anderson Cancer Center and the University of Texas at Austin. Those patients considered eligible included those over the age of 18 who were not pregnant, who had a history of normal menses and no history of an abnormal Pap smear. Patients were consented by a research nurse and underwent a demographic interview, risk factor questionnaire, complete history and physical exam, and pan-colposcopy of the vulva, vagina, and cervix. Patients additionally underwent a urine pregnancy test, chlamydia and gonorrhea cultures, a Papanicolaou smear, and Virapap testing (DiGene, Bethesda, MD) as well as HPV DNA and mRNA sampling. Patients were entered into the study at any time during the menstrual cycle. Blood was drawn for FSH, estradiol, and progesterone levels. The last menstrual period and menstrual history were asked of each patient.

The patients were then followed throughout one menstrual cycle. Three colposcopically normal sites were chosen by one of the investigators (MF) at one of the 12 o'clock positions possible with 12 o'clock being directly above the os. These locations were noted and fluorescence EEMs were measured daily from these three sites. The cervix has both columnar and squamous epithelium, and each site was categorized as squamous or columnar epithelium. The patients were asked about their menstrual bleeding, and it also was noted daily by examination by the research nurse. For the purposes of analysis, the menstrual cycle was divided into four phases: the proliferative phase (which precedes ovulation), ovulation, the secretory phase (following ovulation), and the menstrual phase (during which bleeding occurs). For each patient, the days on which bleeding was observed were assigned to the menstrual phase of the cycle. Ovulation was assumed to occur at cycle day 14, with the preceding days assigned to the proliferative phase of the cycle and the following days assigned to the secretory phase of the cycle. At the end of the study a Papanicolaou smear was taken from each patient, and three biopsies were taken from eight of the ten patients.

2.2 Instrumentation

The spectroscopic system used to measure fluorescence excitation-emission matrices (EEMs) has been described previously [19]. The system measures fluorescence emission spectra at 16 excitation wavelengths, ranging from 330 nm to 480 nm in 10 nm increments with a spectral resolution of 7 nm and incorporates a fiber optic probe, a Xenon arc lamp coupled to a monochromator to provide excitation light, and a polychromator and thermo-electrically cooled CCD camera to record fluorescence intensity as a function of emission wavelength. Figure 1 shows a block diagram of the system.

2.3 Measurements

To provide a negative control, a background EEM was obtained with the probe immersed in a non-fluorescent bottle filled with distilled water at the beginning of each day. Following this, a fluorescence EEM was measured with the probe placed on the surface of a quartz cuvette containing a solution of Rhodamine 610 (Exciton, Dayton, OH) dissolved in ethylene glycol (2 mg/mL) at the beginning of each patient measurement. In order to correct for the non-uniform spectral response of the detection system, the spectra of two calibrated sources were measured at the beginning of the training and validation phases of the study; for the visible a NIST traceable calibrated tungsten ribbon filament lamp was used, and for the UV a deuterium lamp was used (550C and 45D, Optronic Laboratories Inc, Orlando, FL). Correction factors were derived from these spectra and the dark-current-corrected EEMs from the subjects were then corrected for the non-uniform spectral response of the detection system. Variations in the intensity of the fluorescence excitation light source at different excitation wavelengths were corrected using measurements of the intensity at each excitation wavelength at the probe tip made using a calibrated photodiode (818-UV, Newport Research Corp.).

Before the probe was used it was disinfected with Metricide (Metrex Research Corp.) for 20 minutes. The probe was then rinsed with water and dried with sterile gauze. The disinfected probe was guided into the vagina and its tip positioned flush with the cervical epithelium. Then fluorescence EEMs were measured from three cervical sites. The measurement of each EEM required approximately two minutes.

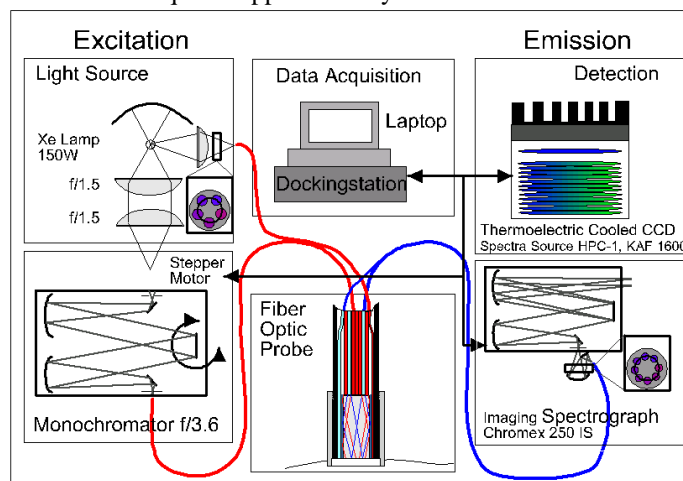


Fig. 1. Block diagram of system used to measure fluorescence EEMs.

2.4 Histological evaluation

Each patient's Papanicolaou smears were reviewed by the study cytologist three times. Eight of the ten patients participated in a second study and underwent colposcopically directed biopsy of the three sites. Study biopsies were also reviewed three times.

2.5 Data Review

Ten subjects were enrolled in and completed this study. The patients ranged in age from 26 to 45. All ten patients were premenopausal as determined by FSH levels, and nine of ten had ovulatory bleeding by medical history and by estradiol and progesterone levels. One patient (patient 2) had anovulatory cycles as evidenced by a prolonged cycle. Nine of the ten Pap smears were within normal limits; one patient had Human Papilloma Virus-associated atypia and Cervical Intraepithelial Neoplasia grade 1 (patient 7). Eight of the ten patients participated in a second study and underwent colposcopically directed biopsies. Seven of eight of these had normal biopsies from each site. The patient with the abnormal Pap smear had the diagnosis confirmed histopathologically.

2.6 Data Analysis

To visualize the changes at each site over the menstrual cycle for each subject we created a sequential arrangement of normalized contour maps (using Matlab, version 6.0 release 12, MathWorks Inc.) to make essentially an animated movie of the EEMs at each site over the menstrual cycle for each woman. The EEM data was log transformed to enhance the visualization of the less-intense sections of the EEM data. The normalization used was identical to that used by Cox et al. [20] (normalizing to the integrated intensity of the NADH peak). The images were rescaled to a maximum of 255 and contour lines were added every five intensity levels. Also, pseudocolor was used to enhance the visualization of subtle intensity changes. The intent of this analysis is to use the advanced flexible (no preconceived relationships assumed between data points) data correlation ability of the human visual system to recognize patterns or trends in visually presented data (images).

3. Results

3.1 Patient Measurements

Each of the ten patients underwent fluorescence EEMs daily from three sites. For seven patients, all three sites were from the squamous epithelium. For three patients, one site was from the columnar epithelium and two sites were from the squamous epithelium. EEMs were measured from 30 total sites, with an average of ~30 (one cycle) sequential measurements per patient for a total of ~900 EEMs. All spectra were reviewed by a two investigators blinded to the pathologic results (UU, RRK) for spectral indications of probe slippage or poor contact. Some of the spectra were determined unusable for analysis and were replaced with blank EEMs (10 out of the ~900 EEMs were so replaced).

3.2 Data Visualization and Interpretation

Individual animations were made that incorporated all of the EEM images from each day of the menstrual cycle for each site in each patient. These animations cover one entire menstrual cycle. Figure 2 is an example of an animation illustrating variations in the normalized EEM throughout the menstrual cycle for a squamous epithelial tissue site. Figure 3 is an example of an animation illustrating variations in the normalized EEM throughout the menstrual cycle for a columnar epithelial tissue site. Along the X-axis are the emission wavelengths; along the Y-axis are the excitation wavelengths. In the lower right-hand corner of all of the images is text that represents the day of the cycle on which the data was acquired. For the menstrual part of the cycle the text is red, for the proliferative phase of the cycle the text changes to yellow, and for the secretory phase of the cycle the text changes to green.

While examining the 30 EEM movies from the ten subjects, we noticed a repeating modification pattern that could be attributed to blood absorption affects. The following series of figures crudely models the effect of blood on a tissue EEM. Figure 4(A) shows a simulated absorption matrix for oxygenated blood (each row is the absorption spectra scaled by the absorption of the excitation wavelength corresponding to the row position, all absorption

coefficients are from <http://www.omlc.org/spectra/hemoglobin/index.html>) and Figure 4(B) shows a simulated absorption matrix for deoxygenated blood. In both of these absorption matrices there appears a noticeable squaring pattern due to wavelengths over which the absorption coefficients are changing rapidly as a function of wavelength. Figure 5 shows the combination of both oxy- and deoxy-hemoglobin. Figure 6 shows an example of cervical-tissue EEM with little or no visual blood absorption effects measured from one of the subjects enrolled in this study.

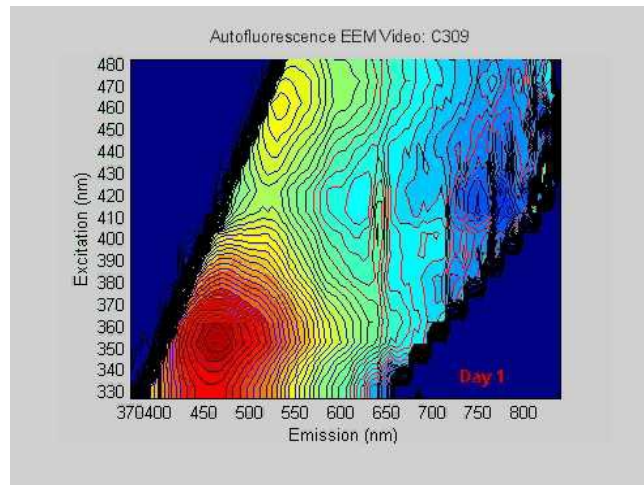


Figure 2. (620KB) Movie of variations in the normalized EEM as a function of cycle date for a squamous normal site from subject 309, site 2.

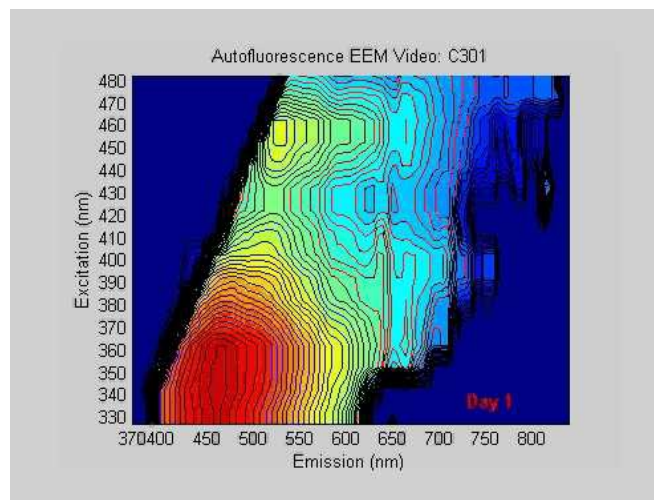


Figure 3. (819KB) Movie of variations in the normalized EEM as a function of cycle date for a columnar normal site for subject 301, site 1.

The contour lines and peaks appear smooth and rounded without any vertical or horizontal bands. When the tissue fluorescence EEM of Figure 6 is divided by the blood absorption matrix of Figure 5 it results in the calculated EEM seen in Figure 7. The general shape of the characteristic tissue peaks is still noticeable, but there is also a significant 'squaring effect' produced by the absorption of hemoglobin. The next EEM, Figure 8, shows a measured EEM

from a cervical site with significant hemoglobin absorption, in which a very similar squaring pattern can be seen. Since the patterns that occur are very distinct, the degree of the blood

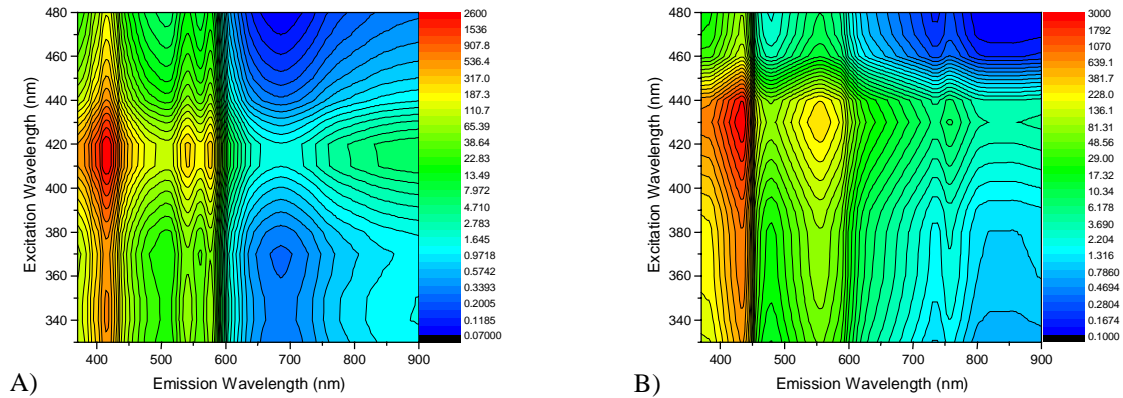


Figure 4. Absorption matrices of A) oxygenated blood and B) deoxygenated blood.

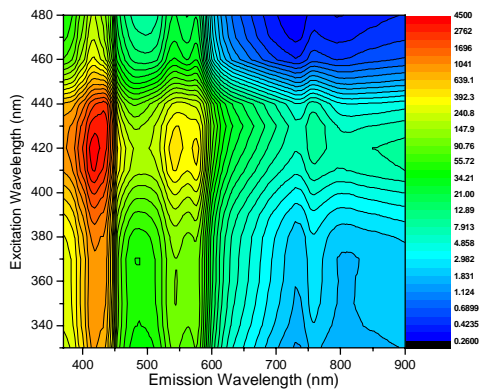


Figure 5. Equally weighted combination of deoxygenated blood and oxygenated blood absorption matrix.

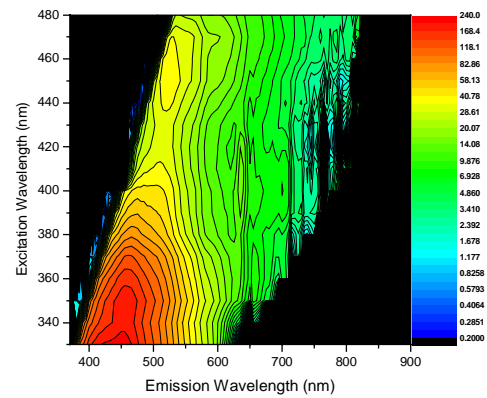


Figure 6. EEM with little or no blood absorption effects visible.

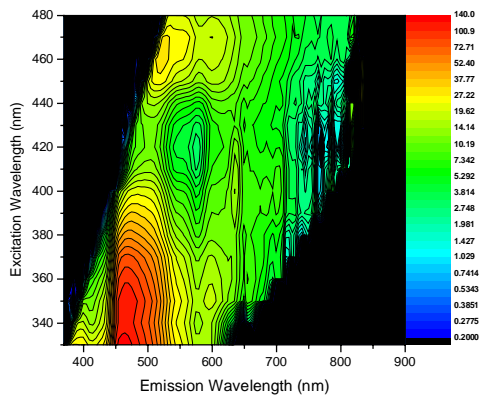


Figure 7. EEM of Figure 6 computationally modified by the blood absorption matrix of Figure 5.

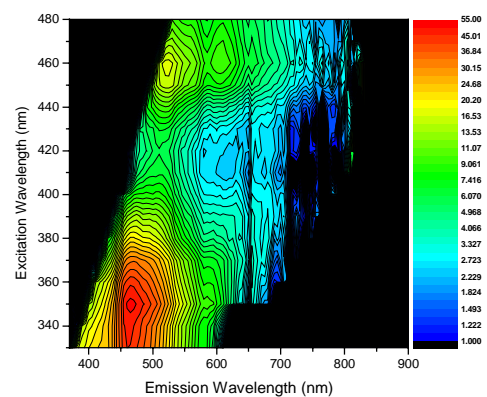


Figure 8. Measured EEM with strong blood absorption effects evident.

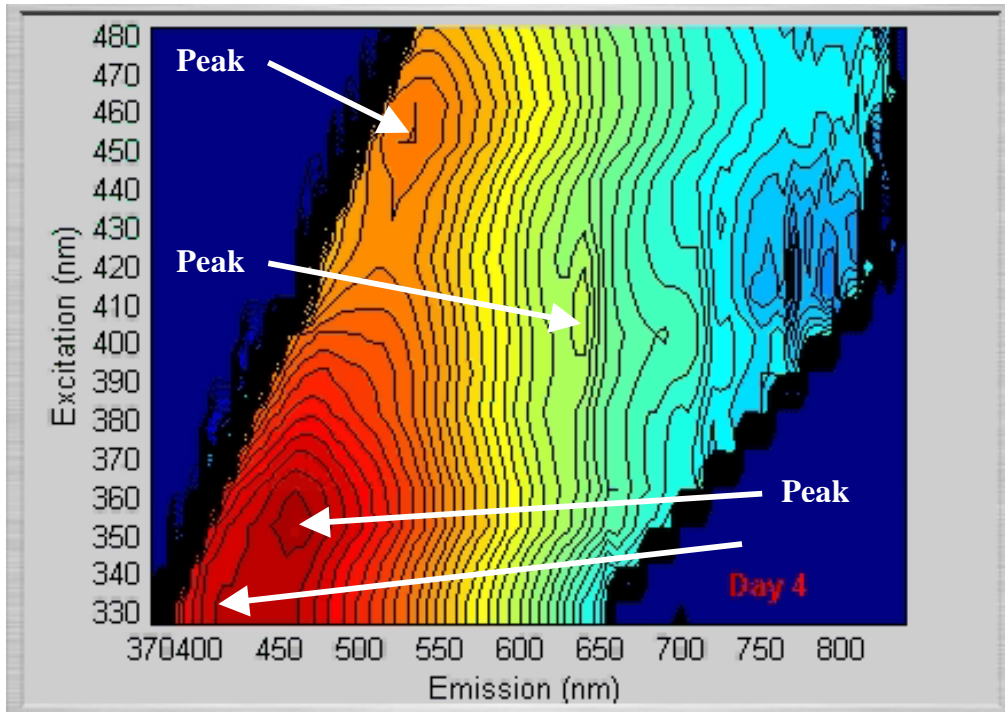


Figure 9. The regions of interest, which were visually assessed in each EEM, are labeled peaks 1-4.

effect could be evaluated by visual examination of the measured EEMs. The degree of this squaring effect is one of the most noticeable differences between the squamous-site animation in Figure 2 and the columnar site animation in Figure 3. Each of the ~900 EEM images was visually examined by one of us (AF) to determine the relative intensity of each of the four peaks shown in Figure 9 as well as to grade the amount of the overall blood effect. Each peak was given a rating of 0 through 10 (0 corresponds to no peak present and 10 to a very strong peak) based upon its visual prominence in the EEM. In a few of the EEMs a remarkably prominent peak could be seen, these instances were denoted with a value of 11. The blood effect was then rated in the same manner. The contour lines aided in determining the strength of a peak since they border changes in intensity level (at 5 count intervals) and indicate the general shape or size of each peak. Refer to Table 1 for an example of this rating system.

Most of the visually perceived features could be rated in a straightforward manner. If there were no closed contour lines (indicating a peak) at an expected peak location, it was assigned a rating of 0. The grading of peak intensities then progressed in numerical order. To identify if there was hemoglobin absorption affecting the EEM the observer examined the overall shape of the contour lines within the EEM (looking for squaring). The amount of squaring of the contour lines and the effect on peaks 1 and 4 determined the visually assigned score for the amount of modification, as modeled in Figure 6 and shown in Figure 8, due to blood absorption in the EEM. This was evident by a general squaring of the contour lines and poor definition of peaks 1 and 4. There could also be attenuation apparent in wavelengths where blood absorption is high, which could produce a very sudden drop in intensity and affect the shape of most of the peaks. As the blood effect became stronger, the squaring was more evident and there was more noticeable attenuation. The size of these observed features and their scored magnitude was much larger than the variability associated with repeat

measurements of the same tissue. A description of the sources of device-dependent EEM variability and their magnitude for the FastEEM can be seen in Bueeler²¹.

This visual scoring data was analyzed to find trends or patterns related to the menstrual cycle. Figure 10 shows a graph of the visually assessed EEM characteristic with the strongest correlation to the day of the menstrual cycle. In Figure 10 the correlation of visually assessed amount of blood absorption for each site in each of the ten subjects is plotted. There does not appear to be any obvious trend in the data across all squamous sites and all subjects over the duration of the menstrual cycle. There is the suggestion of a decreasing amount of blood absorption as a function of the day of cycle in a few of the graphs (subject 309 site1, subject 310 sites 1 and 3, subject 305 site 2, subject 308 site 1 and subject 307 site 1) but nothing definitive. In this Figure, the subjects were ordered from the youngest to oldest (left to right) to see if there are age-related effects in the visual trends.

Table 1: Example of the Visual Estimation of Feature Strength for Site 1 of Subject C300

DAY	SITE	PEAK 1	PEAK 2	PEAK 3	PEAK 4	BLOOD
1	1	10	6	4	8	10
2	1	10	6	4	8	10
3	1	10	6	2	8	8
4	1	10	6	2	8	8
5	1	10	7	0	8	5
6	1	10	6	2	11	8
7	1	10	6	0	9	8
8	1	10	6	2	6	6
9	1	10	7	2	8	8
10	1	10	7	2	8	6
11	1	10	6	2	11	10
12	1	10	6	2	11	8
13	1	10	7	2	10	8
14	1	10	4	4	8	4
15	1	10	7	2	8	6
16	1	10	7	2	8	6
17	1	10	8	2	11	8
18	1	10	7	0	8	8
19	1	10	7	0	8	8
20	1	8	8	0	10	2
21	1	10	7	0	8	2
22	1	10	6	0	8	2
23	1	8	8	2	10	10
24	1	10	6	0	8	4
25	1	10	4	1	6	2
26	1	10	2	0	6	2
27	1	10	6	0	6	2
28	1	N/A	N/A	N/A	N/A	N/A

Only the first 28 days of the menstrual cycle are plotted for each subject. While there appear to be individual trends for some subjects at some sites, there does not appear to be any trends that are consistent across all subjects and sites. In particular, peak 1, peak 2, peak 3, and peak 4 were even more random in their relationship with day of menstrual cycle or other visually assessed features (graphs not shown) than the feature shown in Figure 10.

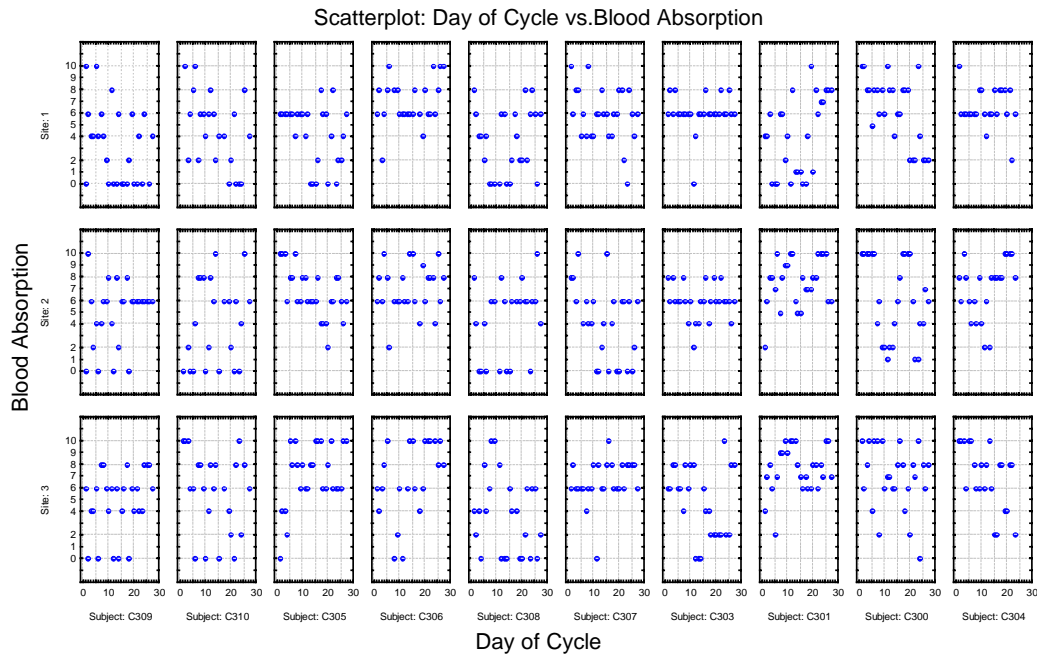


Figure 10. Correlation of visually assessed amount of blood absorption for each site in each of the ten subjects. Patients ordered by increasing age. Columnar sites: subject C301 site 1, subject C306 site 3 and subject C310 site 2.

To further visually search for systematic associations of EEM features with the menstrual cycle, the data was organized into a temporal series of EEMs (varying in duration from 23 days for subject C304 to 38 days for subject C301) for each individual patient and site. These site-specific temporal EEM data series for each patient were resampled using a linear interpolation to generate a time standardized 28-day menstrual cycle EEM time series for each site for each patient. Selecting out only the squamous sites, these time-standardized, site-specific data sets were reorganized such that an average EEM across all sites for each individual day of the time-standardized 28 days was calculated. This resulted in a squamous average EEM time series for a standardized 28-day menstrual cycle (denoted as the standardized 28-day mean EEM time series).

These 28 individual daily average EEMs were then in turn averaged together to generate an average squamous EEM for these ten volunteers, as shown in Figure 11. To examine the visual changes in the EEMs over the menstrual cycle the average EEM of Figure 11 was subtracted from each day of the standardized 28-day mean EEM time series to generate a residual EEM time series. The 28-day residual EEM time series (scaled by 5X to ease visualization) can be seen in Figure 12. There does not appear to be a consistent pattern to the residual over the duration of the cycle or over limited sequential subsets of the cycle. The most consistent pattern in the residual appears in days 1 to 5 in which a strong blood absorption pattern can be seen as evidence by the squaring pattern similar to that described earlier. The area of blood absorption modification seen in the first five days of the animation in Figure 12 overlaps an area of intense signal in the average image (Figure 11, excitation wavelengths 340nm to 360nm, emission wavelengths 420nm to 440nm), making this observed pattern unlikely to be due to noise in the EEMs. In an independent purely statistical analysis, the only area found to have a significant statistical correlation with the day of the

menstrual cycle in Cox et al.²⁰, after correction for multiple comparisons was the area, excitation wavelengths 340nm to 370nm, emission wavelengths 420nm to 445nm. This corresponds well with the area of the strongest peak in the EEM modified by blood absorption as seen in Figure 12.

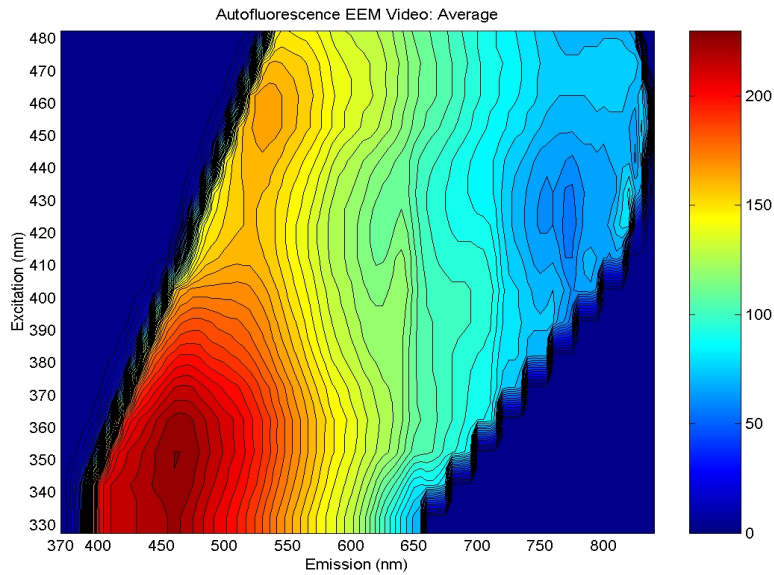


Figure 11: Average EEM for all the squamous sites across all ten subjects.

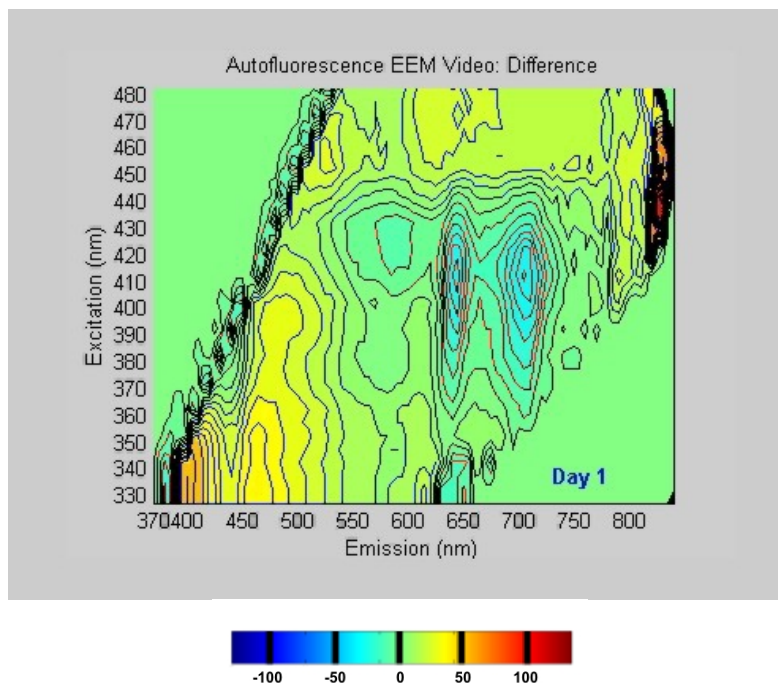


Figure 12: (558KB) Movie of the 28-day residual EEMs time series. Intensity values have all been magnified by a factor of 5X

4. Discussion and conclusions

This study visually assessed the appearance of EEMs from ten women volunteers, where the same three sites were measured from each patient sequentially over their menstrual cycle. For each site, these sequential EEMs were ordered by day of the patient's menstrual cycle and combined to form an EEM animation for each site. These movies were then analyzed visually to see if any pattern linked to the menstrual cycle could be observed. While no consistent pattern was observed, some striking visual features were seen. Features in the EEMs consistent with blood absorption were observed. A simple mathematical simulation was constructed to model the effect of blood absorption on measured EEMs. Visually the model was found to generate EEMs similar to those observed, which are likely due to blood absorption. This extremely simple forward model assumed that the interaction of the excitation light and the emission light with hemoglobin chromophores occurred in exactly the same fashion (similar optical paths for all the excitation light wavelengths and the emitted light). A more realistic and much richer possible backward or forward model would be to allow the amount of excitation light absorption to smoothly vary around the basic hemoglobin absorption profile to reflect the properties of the optical path(s) of the excitation light. Such a model might allow one to infer at what depth(s) within the tissue the majority of the hemoglobin absorption is occurring and the relative tissue-depth relationship of the fluorophores relative the hemoglobin.

It had been noted in previous work that there is substantial variability in the autofluorescence spectra within sites recorded to have equivalent pathological characteristics (all of the same pathology grade). We investigated whether this variability was in some repeatable, predictable way linked to the day of the patient's menstrual cycle. Based on the visual interpretation of the ~900 EEMs from these ten women, this does not appear to be the case, or if such systematic behavior is present, it is masked by the day-to-day and site-to-site variability within these ten subjects. Changes in signals from porphyrin, NADH, and FAD fluorescence and blood absorption were noted when the data was viewed in a graphical format. Blood absorption features were more prominent during the menstrual phase, suggesting that measurements during this phase should be avoided. More quantitative mathematical- and statistical-analysis approaches to the variability present in the data set have reached similar conclusions [20, 22] that there does not appear to be much correlation between the data encapsulated in the EEMs and the day of the menstrual cycle. In summary, variations in cycle data likely do not account for inter- or intra-patient variations.

Acknowledgments:

We gratefully acknowledge Gregg Staerkel for cytological review and Anais Malpica for histopathological review. This work was funded as part of NIH Program Project Award CA82710.